



**HAL**  
open science

## Functionalization of Carbon Nanotubes with Nickel Cyclam for the Electrochemical Reduction of CO<sub>2</sub>

Silvia Pugliese, Ngoc Tran Huan, Jeremy Forte, Domenico Grammatico, Sandrine Zanna, Bao-Lian Su, Yun Li, Marc Fontecave

► **To cite this version:**

Silvia Pugliese, Ngoc Tran Huan, Jeremy Forte, Domenico Grammatico, Sandrine Zanna, et al.. Functionalization of Carbon Nanotubes with Nickel Cyclam for the Electrochemical Reduction of CO<sub>2</sub>. ChemSusChem, 2020, 10.1002/cssc.202002092 . hal-03034395

**HAL Id: hal-03034395**

**<https://hal.sorbonne-universite.fr/hal-03034395>**

Submitted on 1 Dec 2020

**HAL** is a multi-disciplinary open access archive for the deposit and dissemination of scientific research documents, whether they are published or not. The documents may come from teaching and research institutions in France or abroad, or from public or private research centers.

L'archive ouverte pluridisciplinaire **HAL**, est destinée au dépôt et à la diffusion de documents scientifiques de niveau recherche, publiés ou non, émanant des établissements d'enseignement et de recherche français ou étrangers, des laboratoires publics ou privés.

1 **Functionalization of Carbon Nanotubes with Nickel Cyclam for the**  
2 **Electrochemical Reduction of CO<sub>2</sub>**

3

4 *Silvia Pugliese,<sup>1,2</sup> Dr. Ngoc Tran Huan,<sup>1</sup> Jérémy Forte,<sup>3</sup> Domenico Grammatico,<sup>2,4</sup> Dr. Sandrine*  
5 *Zanna<sup>5</sup>, Prof. Bao-Lian Su,<sup>2</sup> Yun Li,<sup>1\*</sup> Prof. Marc Fontecave<sup>1\*</sup>*

6

7 1. Laboratoire de Chimie des Processus Biologiques, UMR CNRS 8229, Collège de France-  
8 CNRS-Sorbonne Université, PSL Research University, 11 Place Marcelin Berthelot, 75231  
9 Paris Cedex 05, France.

10

11 2. Laboratory of Inorganic Materials Chemistry (CMI), University of Namur, 61 rue de Bruxelles,  
12 B-5000 Namur, Belgium

13

14 3. Sorbonne Université, Institut Parisien de Chimie Moléculaire, UMR 8232 CNRS, 4 place  
15 Jussieu, 75252 Paris Cedex 5, France

16

17 4. Bio-inspired Materials Group: Functionality & Self-assembly, Université de Pau et des Pays  
18 de l'Adour, E2S UPPA, CNRS, IPREM UMR 5254, 64000, PAU, France

19

20 5. Chimie ParisTech-PSL Research University-CNRS, Institut de Recherche de Chimie Paris  
21 (IRCP), 11 rue Pierre et Marie Curie, 75005 Paris, France

22

23 \* to whom correspondence should be addressed : [yun.xu-li@college-de-france.fr](mailto:yun.xu-li@college-de-france.fr);  
24 [marc.fontecave@college-de-france.fr](mailto:marc.fontecave@college-de-france.fr)

25

26 **KEYWORDS:** CO<sub>2</sub> electroreduction; nickel cyclam; pyrene; heterogenization; carbon nanotubes

27

28 **Abstract**

29

30 The exploitation of molecular catalysts for CO<sub>2</sub> electrolysis requires their immobilization on the  
31 cathode of the electrolyzer. As an illustration of this approach, a Ni-cyclam complex, with a  
32 cyclam derivative functionalized with a pyrene moiety, was synthesized, shown to be a selective  
33 catalyst for CO<sub>2</sub> electroreduction to CO and immobilized on a carbon nanotube-coated gas diffusion  
34 electrode by using a non-covalent binding strategy. The as-prepared electrode is efficient, selective,  
35 robust for electrocatalytic reduction of CO<sub>2</sub> to CO. Very high turnover numbers (ca. 61460) and  
36 turnover frequencies (ca. 4.27 s<sup>-1</sup>) were enabled by the novel electrode material in organic solvent-  
37 water mixtures saturated in CO<sub>2</sub>. This material provides an interesting platform for further  
38 improvement.

## 39 Introduction

40

41 Catalysis for CO<sub>2</sub> electroreduction into energy-dense products, such as CO, formic acid,  
42 hydrocarbons and alcohols, has attracted extensive research attention during the last 10 years as this  
43 reaction represents one of the most promising strategies for both CO<sub>2</sub> utilization as a carbon source  
44 and storage of intermittent renewable energy in the form of stable chemical energy. Catalysts are  
45 needed to overcome important kinetic limitations related to the multi-electron and multi-proton  
46 transfers associated with the CO<sub>2</sub> reduction reaction (CO<sub>2</sub>RR). Current research focuses on both  
47 heterogeneous materials<sup>[1-3]</sup> and homogeneous organometallic complexes.<sup>[4, 5]</sup> The former are  
48 favored industrially due to more facile product separation and catalyst regeneration and recovery.  
49 However, molecular compounds afford the opportunity to more easily design and synthetically tune  
50 the coordination environment of the active metal center. Mechanistic studies are also facilitated in  
51 that case. To reconcile these two approaches, homogeneous catalysts can be immobilized on  
52 heterogeneous conductive supports to generate cathode materials for electrolyzers. Such  
53 heterogenized molecular systems thus combine the advantages of a solid material (easy recovery of  
54 products and catalysts, efficient electron transfer from the electrode support to the catalyst, high  
55 Turnover Numbers) with those of molecular complexes (synthetic control of the electronic  
56 properties and the coordination environment of the active sites), while suppressing deactivation  
57 processes (such as dimerization) and solubility issues associated with the latter. This class of hybrid  
58 catalysts for CO<sub>2</sub>RR has been recently described in different review articles.<sup>[6-8]</sup>

59 Among various methods, a widely used and straightforward technique for immobilizing molecular  
60 catalysts is based on hydrophobic and  $\pi$ - $\pi$  stacking interactions between a carbon-based support,  
61 generally graphite electrodes or multi-walled carbon nanotubes (MWCNTs), and the molecular  
62 catalyst, as recently reviewed.<sup>[6-8]</sup> MWCNTs have the advantages of stability, high electrical  
63 conductivity and high surface area. While there have been some successes regarding heterogeneous  
64 immobilization of CO<sub>2</sub>RR catalysts on carbon supports such as MWCNTs, these are few and  
65 limited mainly to polyaromatic macrocyclic ligands.<sup>[8]</sup> For example, immobilization of a CO<sub>2</sub>RR  
66 molecular catalyst is possible without any functionalization of the ligand when the ligand is highly  
67 conjugated as in the case of metal porphyrins and phthalocyanines.<sup>[9-11]</sup> In contrast, when the ligand,  
68 such as bipyridine or benzene-based pincer derivatives, has a limited electronic delocalized  
69 structure, an aromatic group, most often pyrene, has to be covalently added to the ligand: the pyrene  
70 group allows tight grafting of the molecular complex on carbon electrode surfaces via  $\pi$ - $\pi$  stacking  
71 interactions. Regarding such simple ligands functionalized with a pyrene group, the most

72 representative reports concern bipyridine-pyrene derivatives used to immobilize a  
73 [Re(bpy)(CO)<sub>3</sub>Cl] complex on a graphite support<sup>[12]</sup> or a [Mn(bpy)(CO)<sub>3</sub>Br] complex on carbon  
74 nanotubes<sup>[13]</sup> as well as a pincer-pyrene ligand used to immobilize an Iridium complex onto a gas  
75 diffusion electrode via carbon nanotubes.<sup>[14]</sup> The three materials displayed interesting  
76 electrochemical CO<sub>2</sub>RR catalytic properties, however in some cases with limited activity and  
77 stability.

78 In order to explore other classes of ligands, in particular non-aromatic in nature, and complexes  
79 based on non-noble metals, we have investigated one of the most studied molecular catalysts for  
80 CO<sub>2</sub>RR, namely [Ni(cyclam)]<sup>2+</sup> with cyclam = 1,4,8,11-tetraazacyclotetradecane. To our  
81 knowledge, while the heterogenization of [Ni(cyclam)]<sup>2+</sup> complex has already been proposed,<sup>[15, 16]</sup>  
82 there is no precedent for its non-covalent immobilization on a carbon-based nanostructured  
83 electrode. For that purpose, we have synthesized an original pyrene-cyclam derivative and the  
84 corresponding Ni complex, complex **1** in Scheme 1, which was found to be a unique 6-coordinated  
85 Ni cyclam complex. We report here the electrocatalytic properties of complex **1** both in solution and  
86 after immobilization on MWCNTS. The complex proved to behave as a very selective  
87 homogeneous catalyst for CO<sub>2</sub> electroreduction to CO in organic solvents in the presence of water.  
88 Furthermore, the presence of a pyrene moiety on the ligand was exploited to readily heterogenize  
89 the complex on MWCNTs via non-covalent interactions. The novel hybrid solid electrode, obtained  
90 by deposition of the functionalized MWCNTs on a Gas Diffusion Layer, was found to be active,  
91 stable and highly selective for CO<sub>2</sub> electroreduction to CO in acetonitrile-water solvent. These  
92 results illustrate the potential of immobilized molecular catalysts for CO<sub>2</sub> electroreduction, a class  
93 of materials yet to be developed for such an application.

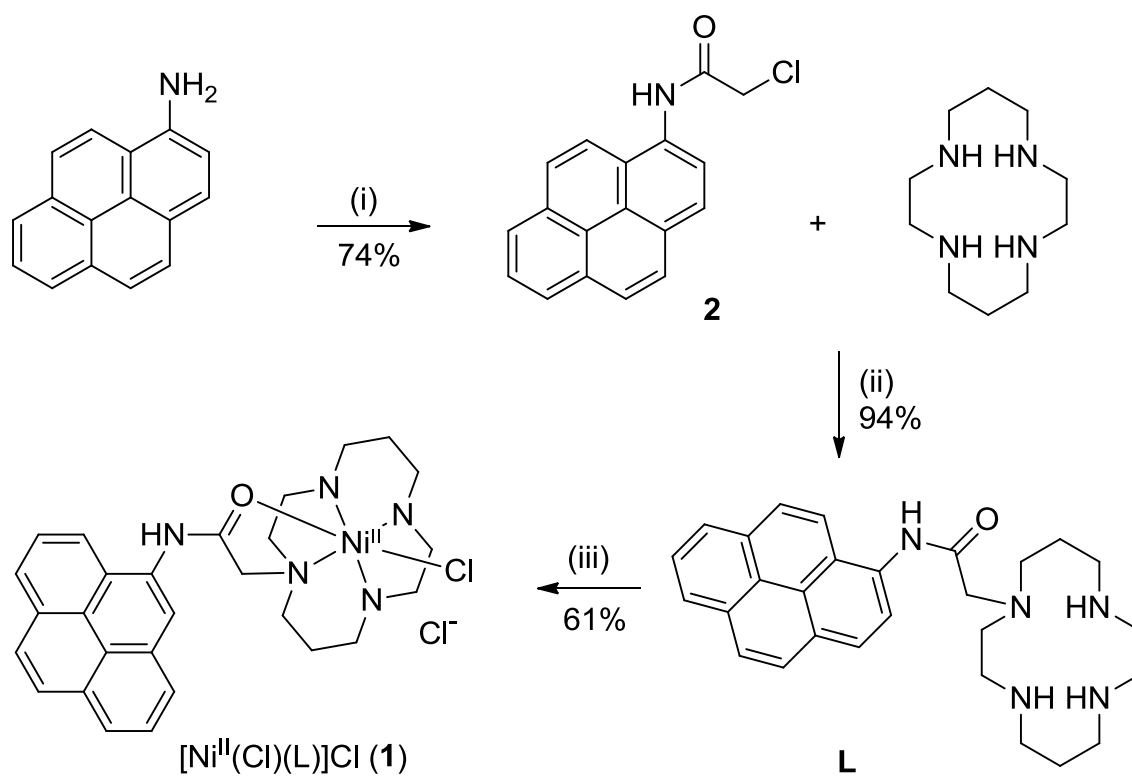
94

## 95 **Results**

96

### 97 *Complex synthesis and characterization*

98



99

100 **Scheme 1.** Synthesis of complex **1**. Conditions: (i)  $\text{ClCH}_2\text{COCl}$ ,  $\text{NEt}_3$ ,  $\text{CH}_2\text{Cl}_2$ ; (ii)  $\text{K}_2\text{CO}_3$ ,  $\text{KI}$   
 101 (cat.),  $\text{CH}_3\text{CN}$ ; (iii)  $\text{NiCl}_2 \cdot 6\text{H}_2\text{O}$ ,  $\text{EtOH}$ .

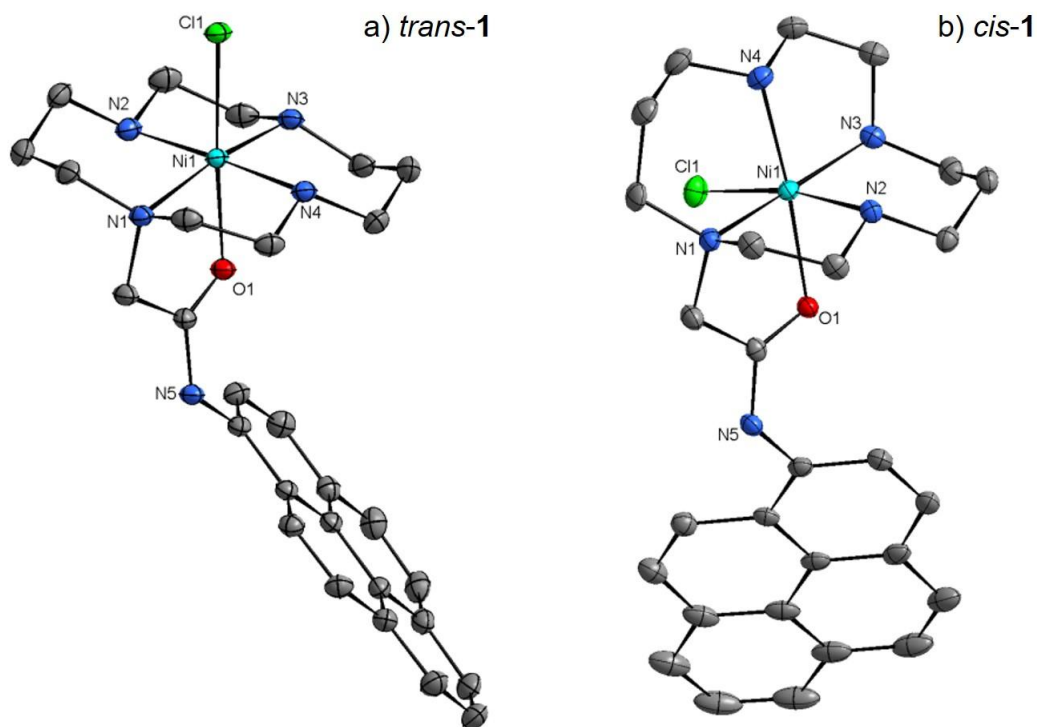
102 In order to synthesize a  $[\text{Ni}(\text{cyclam})]^{2+}$  complex bearing a pyrene group, we chose to prepare the  
 103 ligand **L**, in which one N atom of the cyclam ring is alkylated with a substituent containing a pyrene  
 104 moiety (Scheme 1), according to a previously reported procedure.<sup>[17]</sup> However, this previous  
 105 synthesis gave the product in low yields and required arduous chromatographic purification. In this  
 106 work, we improved the experimental procedure, especially for the N-alkylation of the cyclam ring  
 107 step, by replacing the chromatographic purification step with washing with water, and **L** could be  
 108 easily synthesized on a large scale. The corresponding nickel complex  $[\text{Ni}^{\text{II}}(\text{Cl})(\text{L})](\text{Cl})$  (**1**) was  
 109 obtained using nickel chloride hexahydrate in ethanol for metallation.

110 Complex **1** was isolated in the form of crystals suitable for X-ray analysis. Crystal data of all  
 111 obtained structures are available in Table S1. Four different solvents, ethanol ( $\text{EtOH}$ ), acetonitrile  
 112 ( $\text{CH}_3\text{CN}$ ), dichloromethane ( $\text{CH}_2\text{Cl}_2$ ) and *N,N*-dimethylformamide (DMF) were used for  
 113 crystallization, resulting in different crystal packings differentially stabilized by intermolecular  
 114 hydrogen bonding,  $\pi$ -stacking and Van der Waals interactions (Table S1). In all structures, the  
 115 nickel center ion was found in a distorted octahedral coordination geometry, with a chloride ion and  
 116 the oxygen atom of the amide carbonyl group occupying two ligand positions and completing the  
 117 four coordinating nitrogen atoms of the cyclam ring. However, two different structures, with

118 different configurations, were obtained, reflecting the presence of two isomers, named *trans-1* and  
119 *cis-1* in the following. Four crystal structures of *trans-1* and two crystal structures of *cis-1* were  
120 solved (Tables S1 and S2). In *trans-1*, which crystallized in all solvents used, Cl and O ligands  
121 occupy the axial positions and are thus *trans* to each other with respect to the Ni ion, while the four  
122 positions of the equatorial plane are occupied by the N atoms of the cyclam ring (Figure 1a). For the  
123 *cis-1* isomer, which crystallized in EtOH and DMF, Cl and O ligands are *cis* to each other: the  
124 equatorial plane is constituted by three N atoms of the cyclam ring (two secondary and one tertiary  
125 amines) and a Cl ligand while the apical positions are occupied by the O atom of the amide  
126 carbonyl group and the fourth N atom (one secondary amine) of the cyclam ring (Figure 1b). In the  
127 two isomers, the nickel ion, the tertiary nitrogen atom and the carbonyl oxygen atom are together  
128 part of a five-membered ring with two carbons from the dangling substituent (Figure 1). Each  
129 isomer is a racemic mixture of two enantiomers (only the *R,S,S,R trans-1* and the *S,S,S,S cis-1* are  
130 shown in Figure 1).

131 Bond lengths and angles values for all obtained crystal structures are given in Table S2. The Ni-O  
132 bond lengths are in the range of those of Ni-N (between 2.05 and 2.14 Å), while the Ni-Cl bond  
133 lengths (between 2.40 and 2.45 Å) are slightly longer. All these values are close to those of a  
134 similar octahedral [Ni(cyclam)(OH<sub>2</sub>)(Cl)]Cl complex, previously reported by Zhanaidarova and al  
135 (Ni-O distance : 2.17 Å and Ni-Cl distance : 2.52 Å).<sup>[16]</sup>

136



137

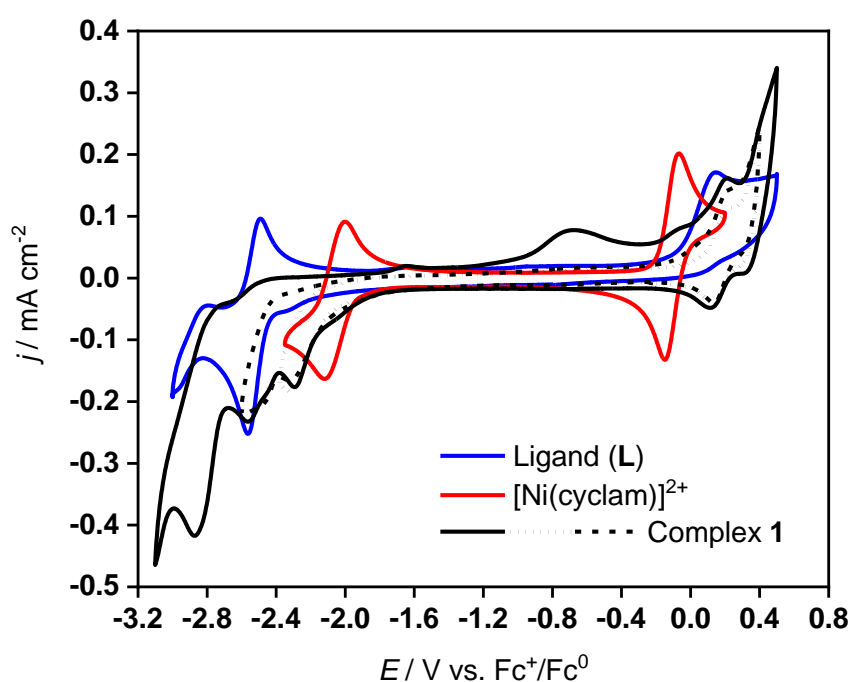
138 **Figure 1.** Crystal structure representation of the cation part of complex **1**. Ellipsoids are drawn with  
139 30% probability. All hydrogen atoms are omitted for the sake of clarity. (a) *R,S,S,R trans-1* (from  
140 crystallization in CH<sub>3</sub>CN); (b) *S,S,S,S cis-1* (from crystallization in DMF). Only one of the  
141 enantiomers is shown in both cases.

142  
143 The electrochemical properties of complex **1** were studied in DMF, with all potentials vs. Fc<sup>+</sup>/Fc<sup>0</sup>.  
144 Figure 2 (dotted, dashed and black) shows the complex cyclic voltammograms (CVs) of complex **1**  
145 (1 mM) in DMF with 0.1 M TBAPF<sub>6</sub> as a supporting electrolyte on a glassy carbon disk (3 mm  
146 diameter) as a working electrode, under an argon atmosphere, when scanned down to either -2.38, -  
147 2.62 or -3.1V. The complexity comes from the fact that two different complexes, *trans-1* and *cis-1*,  
148 are present in solution and that the ligand itself is redox-active due to the presence of pyrene.<sup>[18]</sup> The  
149 first feature at -2.28 V was assigned to the one-electron reduction of Ni<sup>II</sup> to Ni<sup>I</sup>, approximately 180  
150 mV more cathodic than for the unfunctionalized [Ni(cyclam)]<sup>2+</sup> complex peaking at -2.1 V (Figure  
151 2, red), in agreement with a much more electron-enriched Ni center in complex **1** due to the  
152 presence of extra electron-donating ligands. As a confirmation of this assignment to the metal site,  
153 this feature was absent on the CV of the unmetallated pyren-cyclam ligand, **L** (Figure 2, blue). This  
154 signal is irreversible in all CVs even when reversing the scan immediately after the reduction peak,  
155 in contrast to that of [Ni(cyclam)]<sup>2+</sup> (Figure 2). This indicates de-coordination of Cl or/and O  
156 ligands upon reduction. Quite often, a small shoulder was present at -2.1 V, likely corresponding to  
157 a very small amount of the complex without Cl/O coordination, likely in equilibrium with complex  
158 **1** in solution. A second complex irreversible feature appeared at slightly more cathodic potential  
159 (from -2.38 to -2.65 V) and proved difficult to assign. It could possibly have contributions in part  
160 from the one-electron reduction of the pyrene ring, even though the pyren-cyclam ligand, **L**,  
161 exhibits a reversible signal in this potential region (Figure 2, blue). Finally, upon scanning down to  
162 below -3.0 V, a signal at -2.86 V was observed and assigned to Ni<sup>I</sup> to Ni<sup>0</sup> reduction. This signal is  
163 indeed absent within the CV of the unmetallated pyrene-cyclam ligand and is also present in the CV  
164 of [Ni(cyclam)]<sup>2+</sup> upon scanning at a potential (- 2.55 V) allowing Ni<sup>I</sup> to Ni<sup>0</sup> conversion (Figure  
165 S1). On the oxidizing return scan, the feature at + 0.2 V, also found in the unmetallated pyrene-  
166 cyclam ligand, is assigned to ligand oxidation (Figure 2). The broad signal at -0.66 V was  
167 exclusively seen after scanning down to a very negative potential, and not when the cathodic scan  
168 was reversed after the second reduction wave at - 2.62 V. This is consistent with Ni<sup>0</sup> species  
169 generated at negative potentials and adsorbing on the surface of the electrode where they get  
170 oxidized to Ni<sup>II</sup> at -0.66 V during the back scan. A similar situation was observed with the



171 unfunctionalized  $[\text{Ni}(\text{cyclam})]^{2+}$  complex when scanning down to very negative potentials (Figure  
172 S1).

173 The cathodic peak current density ( $j_p$ ) at -2.28 V varied linearly with the square root of the scan rate  
174 ( $v^{1/2}$ ) from 0.01 to 0.5  $\text{Vs}^{-1}$  under Ar, consistent with diffusion-controlled processes and thus with  
175 active complex **1** remaining in solution (Figure S2). We also verified that no adsorption of the  
176 complex occurred at the surface of the GC electrode. Indeed, when, after 30 cycles of CV, the  
177 electrode was removed from the electrolyte and used in a fresh electrolyte without complex **1**, no  
178 signal corresponding to complex **1** could be observed in the CV.



179

180 **Figure 2** Cyclic voltammograms of complex **1** (black, dashed and dotted),  $[\text{Ni}(\text{cyclam})]^{2+}$  (red),  
181 ligand (**L**, blue). Conditions: DMF with 0.1M  $\text{TBAPF}_6$  as the electrolyte, under Ar and at room  
182 temperature. Concentrations were 1 mM for all species. Scan rate  $100 \text{ mV s}^{-1}$ .

183

184  *$\text{CO}_2$  reduction catalyzed by complex 1*

185

186 Upon addition of  $\text{CO}_2$ , in the absence of a source of protons, the CV of 1 mM complex **1** (Figure  
187 S3) presented a small catalytic wave with an increase of current density and a potential at half-peak  
188 catalytic current of about -2.16 V, more anodic that of the  $\text{Ni}^{\text{II}} / \text{Ni}^{\text{I}}$  signal and with an onset

189 potential close to that of  $[\text{Ni}(\text{cyclam})]^{2+}$ . In line with previous reports on  $\text{CO}_2$  electroreduction  
190 catalyzed by  $[\text{Ni}(\text{cyclam})]^{2+}$ , this wave is assigned to the catalytic reduction of  $\text{CO}_2$  to CO during  
191 which reduction of  $\text{Ni}^{\text{II}}$  to  $\text{Ni}^{\text{I}}$  promotes de-coordination of Cl/O ligands and allows  $\text{Ni}^{\text{I}}$  to bind and  
192 activate  $\text{CO}_2$  within a liberated coordination site.<sup>[19]</sup>

193 However, given the importance of protons in the  $\text{CO}_2\text{RR}$  in general and specifically for  $\text{CO}_2\text{RR}$   
194 catalyzed by  $[\text{Ni}(\text{cyclam})]^{2+}$ ,<sup>[20]</sup> the effect of increased concentrations of  $\text{H}_2\text{O}$  was studied by CV  
195 and bulk electrolysis. As expected, the catalytic current increased further upon addition of  $\text{H}_2\text{O}$ ,  
196 from 0.4 M to 2 M (Figure S4a). Considering a  $\text{CO}/\text{CO}_2$  reduction potential in a DMF–water  
197 solvent mixture at - 1.41 V vs.  $\text{Fc}^+/\text{Fc}^0$  ( $\text{CO}/\text{CO}_2$  potential is reported to be - 0.690 V vs. NHE<sup>[21]</sup>  
198 and the  $\text{Fc}^+/\text{Fc}^0$  potential is reported to be 0.720 V vs. NHE in DMF,<sup>[22]</sup> the observed onset potential  
199 at -1.95 V corresponds to an overpotential of about 540 mV. In the absence of  $\text{CO}_2$ , a catalytic  
200 current, assigned to proton reduction to hydrogen, also increased upon increasing the concentration  
201 of  $\text{H}_2\text{O}$  (Figure S4b), however with an onset potential more cathodic than that for  $\text{CO}_2$  reduction.  
202 This reflects the greater potential of complex **1** to catalyze the reduction of  $\text{CO}_2$ . Catalysis was  
203 similarly stimulated when using 2,2,2-Trifluoroethanol (TFE) as a proton source (Figure S5). In the  
204 following, only  $\text{H}_2\text{O}$  was considered as the proton source.

205 A controlled-potential electrolysis (CPE) was then carried out at -2.39 V during which reaction  
206 products were analyzed and quantified, either by gas chromatography (for CO and  $\text{H}_2$ ), by Ionic  
207 Exchange Chromatography (for HCOOH) and  $^1\text{H}$  NMR (for  $\text{CH}_3\text{OH}$ ). For that purpose, the  
208 electrochemical cell used a  $1\text{ cm}^2$  GC plate as the working electrode and the electrolyte was a  
209 solution of complex **1** (1 mM) in  $\text{CO}_2$ -saturated DMF containing 0.1 M  $\text{TBAPF}_6$  and 2 M  $\text{H}_2\text{O}$  as a  
210 proton source. CVs obtained with such a cell reproduced nicely the above CVs (Figure S6a). After  
211 60 minutes electrolysis (Figure S6b), CO was found as the only reaction product in the gaseous  
212 phase (faradaic yield: 96%) and no formate could be detected in the liquid phase. The catalyst  
213 proved quite robust during 1 hour electrolysis as shown from the stability of the current density,  
214 while its activity is limited as shown by the low current density ( $0.3\text{ mA}\cdot\text{cm}^{-2}$ ). As a further proof of  
215 the stability of the catalyst, a CV recorded after CPE was found to be comparable to that before  
216 electrolysis, except for a small decrease in intensity (Figure S6a). The same experiment but in the  
217 absence of complex **1** did not yield any  $\text{CO}_2$  reduction products.

218

219 *Immobilization of complex 1: preparation of the hybrid electrode and characterization*

220

221 Complex **1** was immobilized on MWCNTs through the establishment of  $\pi$ - $\pi$  stacking interactions  
222 between the pyrene moieties and graphene motifs. In the first step, MWCNTs (2 mg) were first  
223 sonicated in ethanol in the presence of Nafion, then drop-casted on a 1 cm<sup>2</sup> surface of commercial  
224 gas diffusion layer (GDL), consisting of a carbon fibres cloth coated with a micro-porous Teflon  
225 layer embedding carbon black so as to keep electronic conductivity properties. Then the  
226 MWCNT/GDL electrode was dipped into a solution of 10 mM complex **1** in DMF, left overnight  
227 and then washed with water and acetonitrile to remove any loosely bound complexes, and finally  
228 air-dried before electrochemical experiments.

229 The **1**/MWCNT/GDL electrode was characterized by Scanning Electronic Microscopy (SEM) and  
230 X-ray photoelectron spectroscopy (XPS). As shown in Figure S7a, a porous network of MWCNTs  
231 was observed in SEM images after functionalization. XPS analysis (survey spectrum) confirms the  
232 presence of Ni and N atoms, from complex **1**, on the surface of the electrode, together with O atoms  
233 from alcohol or carboxylic acid defects of pristine MWCNTs (Figure S8 and Table S3). A Ni 2p<sub>3/2</sub>  
234 signal is observed at 855.9 eV in good agreement with the presence of a Ni<sup>II</sup> ion. Since there is  
235 fluoride in the deposited materials coming from Nafion with the F auger peak masking the Ni 2p  
236 signal at 861.47 eV, a control MWCNT/GDL electrode in the absence of complex **1** has been also  
237 analysed by XPS. The peak decomposition allowed to identify the signal of Ni 2p (Figure S8 and  
238 Table S1) and the ratio of N/Ni is 4.5 approximately, whereas the N 1s peak was centered at 400.4  
239 eV.

240 The **1**/MWCNT/GDL electrode was also characterized by Cyclic Voltammetry. CVs were recorded  
241 in CH<sub>3</sub>CN containing 0.1M TBAPF<sub>6</sub>, using such **1**/MWCNT/GDL electrode (Figure S9). The high  
242 capacitive currents observed in the voltammograms are explained by the 3D structure and the high  
243 surface area of the working electrodes. Integration of the signal at - 1.7 V vs. Fc<sup>+</sup>/Fc<sup>0</sup>  
244 corresponding to Ni reoxidation from Ni<sup>I</sup> to Ni<sup>II</sup> allowed to determine a concentration of  
245 electroactive species for the complex of 5 10<sup>-9</sup> mol cm<sup>-2</sup> (see experimental section). Such a value is  
246 in line with previously reported values for MWCNTs functionalized with molecular Ni  
247 complexes.<sup>[23]</sup> The intensity of that peak was directly proportional to the scan rate, thus confirming  
248 the immobilization of the nickel complex onto the electrode surface (Figure S9).

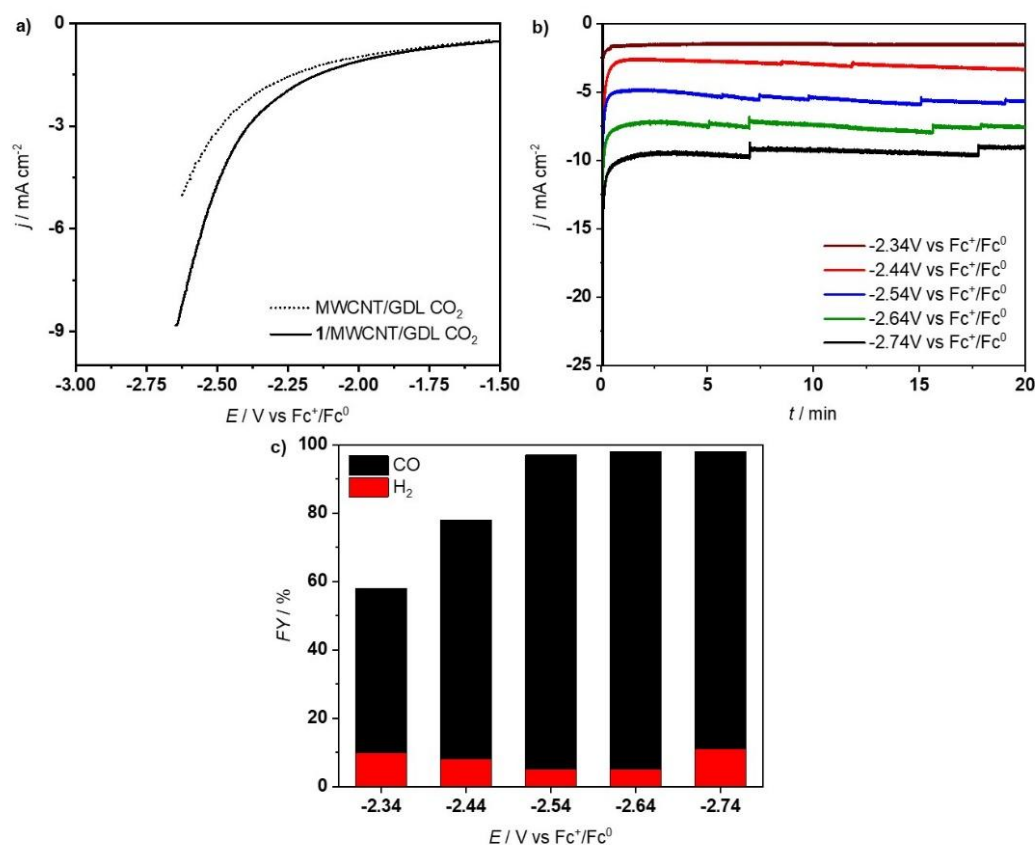
249

250 *Immobilization of complex 1: electroreduction of CO<sub>2</sub>.*

251

252 The electrochemical reduction of CO<sub>2</sub> using the new electrode material was carried out in CH<sub>3</sub>CN  
253 containing 0.1M TBAPF<sub>6</sub> as the electrolyte, in the presence of 1% H<sub>2</sub>O as a proton source, after

254 saturation with CO<sub>2</sub>. A linear sweep voltammogram (LSV) shows a catalytic wave occurring at  
 255 more anodic potentials as compared to the MWCNT/GDL control electrode (Figure 3a).  
 256 Chronoamperometric measurements were carried out at various potentials from - 2.34 to - 2.74 V  
 257 vs. Fc<sup>+</sup>/Fc<sup>0</sup> for 20 min (Figure 3b). The current density proved stable in all cases. As a matter of  
 258 fact, the same electrode could be used for several independent electrolysis experiments without any  
 259 loss of activity. The CO<sub>2</sub> reduction products distribution, in terms of faradaic yields (FY), is shown  
 260 in Figure 3c. CO was the major product at all potentials, with the highest FY value (92%) obtained  
 261 at - 2.54 V vs. Fc<sup>+</sup>/Fc<sup>0</sup> (with a current density of 6 mA.cm<sup>-2</sup>). In all cases H<sub>2</sub> accounted for less than  
 262 11% and no formate could be detected. As a control experiment, CPE using a MWCNT/GDL  
 263 electrode was performed at - 2.54 V vs. Fc<sup>+</sup>/Fc<sup>0</sup> during 20 min (Figure S10a). Not only the current  
 264 density was much lower (2.3 mA.cm<sup>-2</sup>) but the system was selective for H<sub>2</sub> production instead (FY=  
 265 83% with a FY for CO of 4%). As a further control experiment, a CPE of 1/MWCNT/GDL at -  
 266 2.54 V vs. Fc<sup>+</sup>/Fc<sup>0</sup> was also run under Ar (Figure S10b). Only H<sub>2</sub> was produced after 20 min with  
 267 no detectable CO<sub>2</sub> reduction products. Finally, CPE experiments were carried out at - 2.54 V vs.  
 268 Fc<sup>+</sup>/Fc<sup>0</sup> for 20 min with increased amounts of water (3% and 5%). As expected, the system became  
 269 much less selective for CO<sub>2</sub> reduction, leading to FY for CO of only 22% and 12%, respectively.



270

271 **Figure 3.** (a) LSV of **1**/MWCNT/GDL (black) and MWCNT/GDL (dotted) in acetonitrile with  
272 TBAPF<sub>6</sub> 0.1 M and H<sub>2</sub>O 1% under CO<sub>2</sub>. Scan rate 10 mV s<sup>-1</sup>. (b) Controlled Potential Electrolysis  
273 using **1**/MWCNT/GDL as the electrode at different potentials under the same conditions. (c)  
274 Faradaic yields for CO and H<sub>2</sub> after 20 min electrolysis at different potentials.

275 A longer experiment (4h) carried out at - 2.54 V vs. Fc<sup>+</sup>/Fc<sup>0</sup> using the **1**/MWCNT/GDL electrode  
276 under CO<sub>2</sub> confirmed the stability of the catalytic material as well of its selectivity with a FY for  
277 CO of more than 90% after 4h electrolysis (Figure S11). SEM (Figure S7b) as well as XPS (Figure  
278 S12) analysis after 4h electrolysis showed no substantial change in the structure of the electrode. In  
279 the XPS spectrum, the Ni 2p signal was identical to that before electrolysis (Figure S12c). The  
280 decomposition of N1s also confirmed the presence of cyclam (N 1s signal at 400.3 eV), while an  
281 additional signal was observed at around 403 eV, typical of quarternary ammonium such as TBA  
282 present in the electrolyte. The ratio of N/Ni was 4.05 approximately, close to the value before  
283 electrolysis.

284 Based on the amount of electroactive sites on the surface of the electrode ( $5 \times 10^{-9}$  mol cm<sup>-2</sup>), a  
285 remarkable Turnover Number for CO formation of 61460 was obtained after 4 h electrolysis,  
286 corresponding to a Turnover Frequency value of 4.27 s<sup>-1</sup>.

287

## 288 Discussion

289 For the sake of immobilizing a [Ni(cyclam)]<sup>2+</sup> complex at the surface of an electrode, a novel  
290 cyclam derivative carrying a pyrene moiety has been readily synthesized. This class of complex has  
291 been chosen not only because [Ni(cyclam)]<sup>2+</sup> is known to be a good, stable and selective molecular  
292 catalyst for CO<sub>2</sub> electroreduction and it is based on a non-noble metal but also because, to our  
293 knowledge, there is only one precedent for carbon electrode surface modification with  
294 [Ni(cyclam)]<sup>2+</sup> [16]. A [Ni(cyclam)]<sup>2+</sup> complex modified with a carboxylic acid group was used to  
295 for grafting onto titanium(zirconium) oxide surfaces but the resulting material was only studied for  
296 its properties in photoelectron transfer.<sup>[15]</sup> The new complex **1** is a 6-coordinated Ni complex, in  
297 which the tetranuclear N-based coordination of the cyclam ring is completed by a chloride anion  
298 and the oxygen atom of the amide group of the dangling substituent, with two different  
299 configurations, *trans* and *cis*, with respect to the relative positions of the Cl and O ligands.  
300 Coordination to a Ni<sup>II</sup> center by the oxygen atom of a pendant amide group has been recently  
301 reported in the case of substituted cyclen complexes of Ni<sup>II</sup>.<sup>[24]</sup> Complex **1** is thus the first  
302 [Ni(cyclam)]<sup>2+</sup> complex carrying a pyrene substituent.

303 Characterization of the electrochemical properties of complex **1** in DMF/H<sub>2</sub>O using a glassy carbon  
304 electrode has revealed the following features. First, upon one-electron reduction of Ni<sup>II</sup> to Ni<sup>I</sup>, the  
305 complex enjoys decoordination of the Cl/O ligand(s); this is very important since the Ni<sup>I</sup> state is the  
306 active species for CO<sub>2</sub> binding and activation, a process that requires a free Ni coordination site.  
307 Second, catalysis for CO<sub>2</sub> electroreduction occurs at the Ni<sup>II</sup> / Ni<sup>I</sup> redox process, as shown by cyclic  
308 voltammetry, which indicates that the mechanism of the reaction catalyzed by complex **1** follows  
309 that of [Ni(cyclam)]<sup>2+</sup>.<sup>[25]</sup> Third, as in the case of [Ni(cyclam)]<sup>2+</sup> CO<sub>2</sub> reduction catalyzed by  
310 complex **1** is very selective for CO production (FY = 96%). Fourth, as expected, the activity is quite  
311 weak, providing only small current densities; indeed, [Ni(cyclam)]<sup>2+</sup> has been shown to be poorly  
312 catalytically active when using a glassy carbon electrode, while the best activities were obtained  
313 using a mercury electrode, on which the complex adsorbs and enjoys an increased reactivity both in  
314 organic and aqueous electrolytes.<sup>[19, 20, 26]</sup>

315 The pyrene-modified complex **1** has been immobilized on carbon nanotube-coated gas diffusion  
316 electrode using a non-covalent approach and the novel electrode, **1**/MWCNT/GDL, has been  
317 characterized electrochemically for CO<sub>2</sub> electroreduction. Under such an heterogenized  
318 configuration, complex **1** retained its high selectivity for CO production (FY above 90%), with H<sub>2</sub>  
319 accounting for less than 15%. More interestingly, it was shown to be much more active in the  
320 immobilized form than under homogeneous conditions: current densities up to 10 mA.cm<sup>-2</sup> could be  
321 obtained as compared to 0.3 mA.cm<sup>-2</sup> for a 1 mM solution of complex **1**. Finally, the derivatized  
322 electrode proved highly stable leading to impressive turnover numbers (61460 after 4 h  
323 electrolysis). This is remarkable since the electrode support is carbon-based and not mercury, so far  
324 the best electrode material for CO<sub>2</sub> electroreduction catalysed by [Ni(cyclam)]<sup>2+</sup>: this might indicate  
325 that the stable interaction between complex **1** and the carbon surface of the MWCNTs specifically  
326 favors the most reactive conformations of the complex and disfavors CO poisoning, CO desorption  
327 being the turnover-limiting step of the catalytic cycle, as does mercury for the soluble  
328 [Ni(cyclam)]<sup>2+</sup> complex.<sup>[20, 26]</sup> As a consequence, complex **1** is one of the very best molecular  
329 catalysts, after immobilization onto an electrode surface, reported so far for CO<sub>2</sub> electroreduction,  
330 as discussed below.

331 The only previous attempt to graft a [Ni(cyclam)]<sup>2+</sup> complex on a solid electrode (in that case a  
332 covalent grafting onto a glassy carbon electrode) was achieved by Kubiak and coworkers, using  
333 electrooxidation of a terminal alkyne attached to the cyclam ring.<sup>[16]</sup> This led to a cathode material  
334 which proved poorly active (with current densities below 1 mA.cm<sup>-2</sup>) and poorly selective for CO<sub>2</sub>  
335 reduction to CO (FY<sub>CO</sub> = 7%; FY<sub>H<sub>2</sub></sub> = 89 %) under potential and solvent conditions comparable to

336 those used here. The present work thus represents a great improvement regarding the utilization of  
337 solid electrodes functionalized with  $[\text{Ni}(\text{cyclam})]^{2+}$ . This is due in great part to the large surface  
338 area and the nanostructuring of the CNTs support which allow a greater density of electroactive  
339 species. As a matter of fact, the 1/MWCNT/GDL electrode is also much more efficient for  $\text{CO}_2$   
340 reduction to CO than a glassy carbon electrode functionalized with a  $[\text{Re}(\text{bpy})(\text{CO})_3\text{Cl}]$  complex  
341 using the same pyrene-dependent approach: the latter could achieve only 58 TONs during 1 hour  
342 electrolysis, after which the activity was lost.<sup>[12]</sup> Finally, the 1/MWCNT/GDL electrode compares  
343 well with and complements the carbon nanotube-coated gas diffusion electrode derivatized with a  
344 molecular iridium pincer dihydride catalyst, which allows high TONs (200000 in 8 hours) of  
345 formate with high selectivity (> 90%) from  $\text{CO}_2$  electroreduction in aqueous electrolytes.<sup>[14]</sup> While  
346 based on a noble metal, the latter is a reference material with respect to carbon electrodes  
347 functionalized with a molecular catalyst for  $\text{CO}_2$  reduction. Indeed, while  $[\text{Mn}(\text{bpy})(\text{CO})_3\text{Br}]$  was  
348 also attached to MWCNTs via  $\pi$ - $\pi$  interactions of a pyrene group, present in a bpy ligand  
349 derivative, with the CNT sidewalls, the resulting material proved much less active (low current  
350 densities), less stable, less selective (giving a mixture of CO and HCOOH together with  $\text{H}_2$  as the  
351 major product) and achieving TONs of about 1500 after 8 h electrolysis under aqueous  
352 conditions.<sup>[13]</sup>

353 In conclusion, the present study confirms the benefits of incorporation of molecular catalysts onto  
354 electrode surfaces using the pyrene-CNT approach for  $\text{CO}_2$  electroreduction. More specifically, it  
355 shows that the  $[\text{Ni}(\text{cyclam})]^{2+}$  complex provides an excellent platform on which further  
356 improvements of hybrid electrodes can be brought.

357

## 358 **Experimental Section**

### 359 *General*

360 All starting materials were commercially available (Sigma and TCI) and were used without further  
361 purification. Solvents were purified by an MBRAUN SPS-800 Solvent Purification System. All  
362 reactions were carried out under air atmosphere unless specified.  $^1\text{H}$  and NMR spectra were  
363 recorded on a Bruker Avance-III 300 NMR spectrometer (300 MHz) at room temperature. UV-Vis  
364 spectra were recorded using a Cary 100 UV-Vis spectrophotometer instrument (Agilent).

365

### 366 *Synthesis of Complex I*

367 **2-Chloro-*N*-pyren-1-yl-acetamide (2)**. The synthesis was carried on as previously described with  
368 slight modifications.<sup>[27]</sup> Under an Ar atmosphere, 1-aminopyrene (5.45 g, 25.1 mmol) and  
369 triethylamine (5.6 mL, 40.1 mmol) were dissolved in CH<sub>2</sub>Cl<sub>2</sub> (500mL), and chloroacetyl chloride  
370 (2.8 mL, 35.1 mmol) was added dropwise via a syringe. After 12 h of stirring under Ar, the  
371 precipitate was filtered, washed with H<sub>2</sub>O and cold CH<sub>2</sub>Cl<sub>2</sub> several times. The crude product was  
372 dried under vacuum over night to yield the product as a pale-grey powder which was used for the  
373 next step without further purification (5.49 g, 74%). <sup>1</sup>H NMR (CDCl<sub>3</sub>, 300 MHz) δ 9.01 (br s, 1H),  
374 8.45 (d, *J* = 8.3 Hz, 1H), 8.21-8.14 (m, 4H), 8.07-7.99 (m, 4H), 4.42 (s, 2H). This spectrum is  
375 identical to the reported one.<sup>[27]</sup>

376 ***N*-Pyren-1-yl-2-(1,4,8,11-tetraazacyclotetradec-1-yl)-acetamide (L)**. This ligand was synthesized  
377 according to a reported method with slight modifications.<sup>[17]</sup> Under an Ar atmosphere, a mixture of  
378 cyclam (3.25 g, 16.2 mmol), 2-chloro-*N*-pyren-1-yl-acetamide (2) (940 mg, 3.2 mmol), K<sub>2</sub>CO<sub>3</sub>  
379 (2.24 g, 16.2 mmol) and KI (270 mg, 1.6 mmol) in CH<sub>3</sub>CN (677 mL) was heated under reflux.  
380 After 24 h, the solvent was evaporated under reduced pressure and the residue was washed with  
381 water and ether several times. The crude product was dried under vacuum overnight to yield the  
382 product as an off-white powder which was used for the next step without further purification (1.46  
383 g, 94%). <sup>1</sup>H NMR (CDCl<sub>3</sub>) δ 11.4 (br s, 1H), 8.27 (d, *J* = 9.3 Hz, 1H), 8.19-7.96 (m, 8H), 3.44 (s,  
384 2H), 2.90 (t, *J* = 5.4 Hz, 2H), 2.80 (m, 8H), 2.42 (t, *J* = 5.1 Hz, 2H), 2.3 (t, *J* = 5.1 Hz, 2H), 2.12 (m,  
385 2H), 1.95 (m, 2H), 1.49 (m, 2H). This spectrum is identical to the reported one.<sup>[17]</sup>

386 **Complex [Ni<sup>II</sup>(Cl)(L)]Cl (1)**. A solution of **L** (100 mg, 0.11 mmol) in EtOH (2 mL) was added  
387 dropwise to a solution of NiCl<sub>2</sub>·6H<sub>2</sub>O (52 mg, 0.11 mmol) in EtOH (2 mL). The pale green solution  
388 turned immediately to orange then dark pink. After 3h at room temperature, the solvent was  
389 evaporated to dryness and the blue-pink solid was dissolved in EtOH (6 mL) and ether was allowed  
390 to slowly diffuse to this solution to give complex **1** as a pink-purple powder (78 mg, 61%). UV-Vis  
391 [DMF]: λ nm (ε, M<sup>-1</sup> cm<sup>-1</sup>): 543 (10.7), 389 (1880), 353 (10920), 343 (15000), 329 (10000), 277  
392 (16300), 266 (11060).

393 Single crystals suitable for X-ray diffraction were obtained by slow diffusion of Et<sub>2</sub>O into a solution  
394 of DMF containing **1** at room temperature. CH<sub>3</sub>CN, EtOH and CH<sub>2</sub>Cl<sub>2</sub> were also used instead of  
395 DMF giving suitable single crystals. CCDC 2021920 (*trans*-**1**, MeCN), 2021925 (*trans*-**1**, EtOH),  
396 2021922 (*trans*-**1**, DMF), 2021923 (*trans*-**1**, DCM), 2021921 (*cis*-**1**, EtOH) and 2021924 (*cis*-**1**,  
397 DMF) contain the supplementary crystallographic data for this paper.

398



399 *Homogeneous Electrochemical Studies*

400 All electrochemical experiments were performed on a VSP300 potentiostat (Bio-Logic Science  
401 Instruments SAS) and were conducted at room temperature in *N,N*-Dimethylformamide (DMF). 0.1  
402 M tetrabutylammonium hexafluorophosphate (TBAPF<sub>6</sub>) was used as the supporting electrolyte. The  
403 cyclic voltammetry (CV) experiments were carried out in a three electrode setup, with a 3 mm  
404 diameter glassy carbon (GC) electrode as a working electrode, which was polished on a polishing  
405 cloth with a 1 μm diamond suspension (Struers), sonicated for 10 seconds, thoroughly rinsed with  
406 ethanol and dried prior to experiments. Platinum wire was used as a counter electrode and was  
407 previously flame annealed. The reference electrode was an Ag/AgCl electrode in a saturated KCl  
408 solution, equipped with a bridge to allow operation in organic solvent. All potentials were calibrated  
409 using the ferrocene/ferrocenium (Fc<sup>+0</sup>) redox couple as an internal standard, which was added in  
410 solution at the end of each measurement. In DMF, E<sub>1/2</sub> (Fc<sup>+</sup>/Fc<sup>0</sup>) = 0.60V vs Ag/AgCl/sat. KCl.  
411 Only the second cycle of all CVs are shown, although no difference in consecutive scans has been  
412 observed.

413 Controlled potential electrolysis (CPE) experiments were carried out in a gas-tight two-  
414 compartment electrochemical cell with two ceramic-PVDF composite membranes (16 μm  
415 thickness, Xuran) separating the anodic and cathodic compartments. The working electrode was a 1  
416 cm<sup>2</sup> glassy carbon plate, the counter electrode was a platinum mesh and the reference electrode was  
417 an Ag/AgCl electrode in a saturated KCl solution, equipped with a bridge to allow operation in  
418 organic solvent. Anolyte and catholyte contained DMF and 2 M of H<sub>2</sub>O as the proton source and  
419 0.1 M of TBAPF<sub>6</sub> as the electrolyte. Only in the catholyte 1 mM of complex **1** was added. Both  
420 solution compartments were saturated with CO<sub>2</sub> during at least 20 minutes before starting the  
421 electrolysis, but no more gas was bubbled during the electrolysis. The experiments were conducted  
422 at room temperature under stirring at the cathode side. The volume of solution held by the cell in  
423 total was 22.6 mL, with ca. 10.6 mL of total headspace volume.

424 Gas products were quantified by gas chromatography (Model 8610C SRI Instruments) equipped  
425 with TCD and FID detectors from 50 μL aliquots of the headspace of the cathode compartments.  
426 Hydrogen (H<sub>2</sub>) and carbon monoxide (CO) were detected by thermal conductivity detector (TCD)  
427 and flame ionization detector (FID), respectively. Liquid products were evaluated using an ionic  
428 exchange chromatograph (Metrohm 883 Basic IC) equipped with a Metrosep A Supp 5 column and  
429 a conductivity detector.

430 The faradaic yields were calculated by quantifying the products in the head-space gas of the  
431 cathodic side, on the basis of Equation 1:

432 
$$\text{Faradaic efficiency} = \frac{N \times F \times n}{Q} \times 100 \quad (1)$$

433 Where  $Q$ ,  $F$ , and  $N$  represented the charge passed through the system (C), Faraday's constant (C  
434 mol<sup>-1</sup>), and moles of H<sub>2</sub>/CO generated, respectively. In the reaction process, 2 moles of electrons  
435 were consumed to produce 1 mole of product, therefore  $n = 2$ .

436

#### 437 *Electrodes preparation and characterization*

438 The electrodes used a 3 cm x 1 cm gas diffusion layer (GDL, AVCarb GDS 3250, Fuel Cell Store)  
439 strip, which was briefly sonicated in EtOH and let dry in air before utilization. MWCNTs (Sigma)  
440 were used after acid treatment as following: the raw MWCNTs material were dispersed in H<sub>2</sub>SO<sub>4</sub> (2  
441 M), sonicated for 1 h at ambient temperature, washed repeatedly with H<sub>2</sub>O, then EtOH and dried in  
442 a vacuum oven at 70°C overnight. This acid treated MWCNTs (2 mg) were sonicated for at least 30  
443 min in EtOH (200 μl) containing a solution of Nafion perfluorinated resin (5 μl of a 5 wt% solution  
444 in mixture of lower aliphatic alcohols containing 5% water). The suspension was then drop-casted  
445 on the GDL (1 cm<sup>2</sup> deposit) and dried in air at 70°C for at least 30 min. Subsequently, the GDL-  
446 MWCNT electrode was immersed in a solution of complex **1** in DMF (10 mM) overnight on an  
447 orbital shaker at low speed. Finally, the electrode was dried, washed with water then acetonitrile  
448 and dried in air.

449 SEM images were acquired using a Hitachi S-4800 scanning electron microscope. X-ray  
450 photoelectron spectra (XPS) were collected using a Thermo Electron Escalab 250 spectrometer with  
451 a monochromated Al K $\alpha$  radiation (1486.6 eV). The analyzer pass energy was 100 eV for survey  
452 spectra and 20 eV for high resolution spectra. The analysed area was 500 mm<sup>2</sup>. The photoelectron  
453 take-off angle (angle between the surface and the direction in which the photoelectrons are  
454 analysed) was 90°. Curve fitting of the spectra was performed with the Thermo Electron software  
455 Advantage. The electroactive sites were calculated through the integration of the oxidation wave in  
456 the CV scan (Figure S9) according to Equation 2:

$$457 \quad \Gamma Ni = \frac{q}{nFA} \quad (2)$$

458 Where  $\Gamma Ni$  is the number of electroactive sites (mol cm<sup>-2</sup>),  $q$  is the charge (C) obtained from the  
459 integration of the oxidation wave,  $n$  the number of electrons in the redox process per Ni center ( $n =$   
460 1),  $F$  is the Faraday constant (96485 C mol<sup>-1</sup>), and  $A$  is the geometrical electrode area (1 cm<sup>2</sup>).<sup>[13]</sup>

461

#### 462 *Heterogeneous Electrochemical Studies*

463 Linear sweep voltammetry (LSV) was performed for each sample before CPE, first under Ar and  
464 successively under CO<sub>2</sub>. Gas was bubbled in the solution for at least 20 minutes before each  
465 experiment. The scan rate was 10 mV s<sup>-1</sup>. CPE experiments were carried out in a gas-tight H-shape

466 cell in which cathode and reference electrode are separated from the anode by an anion exchange  
467 membrane (AMV Selemion, ACG Engineering). The solvent used was acetonitrile containing 1%  
468 of H<sub>2</sub>O, and the electrolyte was TBAPF<sub>6</sub> 0.1 M. The cathode used was a GDL on which MWCNs  
469 with the complex **1** were drop-casted as described above, the anode was platinum and the reference  
470 electrode was an Ag/AgCl electrode in a saturated KCl solution, equipped with a bridge to allow  
471 operation in organic solvent. All potentials were calibrated using the ferrocene/ferrocenium (Fc<sup>+0</sup>)  
472 redox couple as an internal standard, which was added in solution at the end of each measurement.  
473 In acetonitrile, E<sub>1/2</sub>(Fc<sup>+</sup>/Fc<sup>0</sup>) = 0.54V vs Ag/AgCl/sat. KCl. CO<sub>2</sub> gas was bubbled in the solution for  
474 at least 20 minutes before each experiment and no more gas was bubbled during the electrolysis.  
475 The experiments were conducted at room temperature and under stirring at the cathode side. The  
476 volume of solution held by the cell in total was 22.6 mL, with ca. 10.6 mL of total headspace  
477 volume.

478 The electrolysis products (hydrogen, CO and formate) were quantified in a similar manner as in the  
479 homogeneous electrochemical studies part. The faradaic yields were calculated by quantifying the  
480 products in the head-space gas of the cathodic side, on the basis of Equation 1 (see above).

481 The following formulas

$$482 \quad TON = \frac{\text{moles of product}}{\text{moles of catalyst}} \quad (3)$$

483 and

$$484 \quad TOF = \frac{TON}{\text{reaction time [s]}} \quad (4)$$

485 were used to calculate Turnover Number (TON) and Turnover Frequency (TOF) values,  
486 respectively.

487

#### 488 **Acknowledgements**

489 *S.P. and D.G. acknowledge financial support from the European School on Artificial Leaf:  
490 Electrodes & Devices (eSCALED). This project has received funding from the European's Union's  
491 Horizon 2020 research and innovation programme under the Marie Skłodowska-Curie grant  
492 agreement No 765376.*

493 *We thank Geoffrey Gontard (Sorbonne Universités) for solving the structure of cis-**1** (DMF).*

494 *We thank Françoise Pillier (Sorbonne Universités) for the SEM images.*

495

496

497 **References**

498

- 499 [1] A. Liu, M. Gao, X. Ren, F. Menga, Y. Yang, L. Gao, Q. Yang, T. Ma, *J. Mater. Chem. A.*  
500 **2020**, *8*, 3541–3562.
- 501 [2] B. Kumar, J. P. Brian, V. Atla, S. Kumari, K. A. Bertram, R. T. White, J. M. Spurgeon, *Catal.*  
502 *Today* **2016**, *270*, 19–30.
- 503 [3] D. Gao, F. Cai, G. Wang, X. Bao, *Curr. Opin. Green Sustain. Chem.* **2017**, *3*, 39–44.
- 504 [4] R. Francke, B. Schille, M. Roemelt, *Chem. Rev.* **2018**, *118*, 4631–4701.
- 505 [5] K. Elouarzaki, V. Kannan, V. Jose, H. S. Sabharwal, J. M. Lee, *Adv. Energy Mater.* **2019**, *9*.
- 506 [6] N. Elgrishi, M. B. Chambers, X. Wang, M. Fontecave, *Chem. Soc. Rev.* **2017**, *46*, 761–796.
- 507 [7] C. Sun, R. Gobetto, C. Nervi, *New J. Chem.* **2016**, *40*, 5656–5661.
- 508 [8] L. Sun, V. Reddu, A. C. Fisher, X. Wang, *Energy Environ. Sci.* **2020**, *13*, 374–403.
- 509 [9] X. M. Hu, M. H. Rønne, S. U. Pedersen, T. Skrydstrup, K. Daasbjerg, *Angew. Chemie - Int.*  
510 *Ed.* **2017**, *56*, 6468–6472.
- 511 [10] Y. Wu, Z. Jiang, X. Lu, Y. Liang, H. Wang, *Nature* **2019**, *575*, 639–642.
- 512 [11] X. Zhang, Y. Wang, M. Gu, M. Wang, Z. Zhang, W. Pan, Z. Jiang, H. Zheng, M. Lucero, H.  
513 Wang, G. E. Sterbinsky, Q. Ma, Y. Wang, Z. Feng, J. Li, H. Dai, Y. Liang, *Nat. Energy*  
514 **2020**.
- 515 [12] J. D. Blakemore, A. Gupta, J. J. Warren, B. S. Brunshwig, H. B. Gray, *J. Am. Chem. Soc.*  
516 **2013**, *17*, 30.
- 517 [13] B. Reuillard, K. H. Ly, T. E. Rosser, M. F. Kuehnel, I. Zebger, E. Reisner, *J. Am. Chem. Soc.*  
518 **2017**, *139*, 14425–14435.
- 519 [14] P. Kang, S. Zhang, T. J. Meyer, M. Brookhart, *Angew. Chemie - Int. Ed.* **2014**, *53*, 8709–  
520 8713.
- 521 [15] G. Neri, J. J. Walsh, C. Wilson, A. Reynal, J. Y. C. Lim, L. Xaoe, A. J. P. White, N. J. Long,  
522 J. R. Durrant, A. J. Cowan, *Phys. Chem. Chem. Phys.* **2015**, *17*, 1562–1566.
- 523 [16] A. Zhanaidarova, C. E. Moore, M. Gembicky, C. P. Kubiak, *Chem. Commun.* **2018**, *54*,  
524 4116–4119.
- 525 [17] N. J. Youn, J. S. Kim, K. C. Song, S. H. Kim, S. Ahn, S. K. Chang, *Bull. Korean Chem. Soc.*  
526 **2005**, *26*, 849–851.
- 527 [18] Y. Zhao, D. Xue, H. Qi, C. Zhang, *RSC Adv.* **2017**, *7*, 22882–22891.
- 528 [19] J. D. Froehlich, C. P. Kubiak, *Inorg. Chem.* **2012**, *51*, 3932–3934.
- 529 [20] J. D. Froehlich, C. P. Kubiak, *J. Am. Chem. Soc.* **2015**, *137*, 3565–3573.
- 530 [21] C. Costentin, M. Robert, J.-M. Savéant, *Chem. Soc. Rev.* **2013**, *42*, 2423–2436.
- 531 [22] S. Creager, *Handbook of Electrochemistry*, ed. C. Zoski Elsevier, Amsterdam, **2007**, p.101.
- 532 [23] P. D. Tran, A. Le Goff, J. Heidkamp, B. Joussetme, N. Guillet, S. Palacin, H. Dau, M.  
533 Fontecave, V. Artero, *Angew. Chemie - Int. Ed.* **2011**, *50*, 1371–1374.

- 534 [24] T. Qiu, G. P. A. Yap, J. Rosenthal, *ACS Appl. Energy Mater.* **2019**, *12*, 8560–8569.
- 535 [25] M. Beley, J. P. Collin, R. Ruppert, J. P. Sauvage, *J. Am. Chem. Soc.* **1986**, *108*, 7461–7467.
- 536 [26] Y. Wu, B. Rudshateyn, A. Zhanaidarova, J. D. Froehlich, W. Ding, C. P. Kubiak, V. S.  
537 Batista, *ACS Catal.* **2017**, *7*, 5282–5288.
- 538 [27] J. H. Kim, A. R. Hwang, S. K. Chang, *Tetrahedron Lett.* **2004**, *45*, 7557–7561.
- 539